Available online at www.sciencedirect.com
SCIENCE DIRECT®
Journal of Sound and Vibration 275 (2004) 1051–1068
JOURNAL OF SOUND AND VIBRATION
www.elsevier.com/locate/jsvi

Flexible robot manipulator path design to reduce the endpoint residual vibration under torque constraints

Kyung-Jo Park*

Division of Mechanical and Automotive Engineering, Faculty of Engineering, Yosu National University, San 96-1, Dun-deok dong, Yosu, Chonman 550-749, South Korea

Received 11 November 2002; accepted 4 July 2003

Abstract

In this work, a new method is presented for generating the path that significantly reduces residual vibration under the torque constraints. The desired path is optimally designed so that the required movement can be achieved with minimum residual vibration. From the previous research works, the dynamic model has been established including both the link and the joint flexibilities. The performance index is selected to minimize the maximum amplitude of residual vibration. The path to be designed is developed by a combined Fourier series and polynomial function to satisfy both the convergence and boundary condition matching problem. The concept of correlation coefficients is used to select the minimum number of design variables, i.e., Fourier coefficients, the only ones which have a considerable effect on the reduction of residual vibration. A two-link manipulator is used to evaluate this method. Results show that residual vibration can be drastically reduced by selecting an appropriate path in both cases of unlimited and torque-limited.

1. Introduction

The need for robot manipulator is increasing to raise the productivity and improve the quality of products in manufacturing industry. Most industrial robots in use today, however, are composed of heavy and stiff links to satisfy the required repeatability and accuracy. These links, therefore, have inherently a large inertia, requiring in turn a long time to complete the motion and more power consumption in the actuators. To increase the productivity by fast motion and to complete a motion with small energy consumption, robot manipulators are required to have light and flexible structures.

*Tel.: +82-61-659-3221; fax: +82-61-659-3220.
E-mail address: kjpark@yosu.ac.kr (K.-J. Park).

0022-460X/$ - see front matter © 2003 Elsevier Ltd. All rights reserved.
doi:10.1016/j.jsv.2003.07.001

If fast motions are performed by light and flexible robot arms, however, the compliance which inherently exists in transmission and structural elements will cause considerable vibration of the robot endpoint at the end of a move. This residual vibration is primarily a result of the additional kinetic energy imparted to the robot by the fast motion. Since structural resonances tend to be lightly damped, any vibration occurring after the final position is reached will require additional settling time before the new task can begin. For that reason, an effective technique to reduce this residual vibration is needed.

Several different approaches have been suggested to reduce residual vibration, which can be loosely categorized as either open-loop or closed-loop strategies. The open-loop strategies consist of specifying force or torque profiles to drive the dynamic system. These have been primarily developed for rotational maneuvers of space structures [1–5]. Closed-loop strategies utilizing constant feedback gains have also been designed for reducing residual vibration of flexible systems. These approaches are to explicitly increase the damping of the flexible modes. Both passive and active methods have been proposed. Alberts et al. [6] added layers of viscoelastic material to a beam in order to add passive damping. Active damping techniques which can be represented as adding distributed damping to beam-like structures have also been proposed. Sliverberg [7] has developed a discrete implementation which approximates uniform distributed damping with several discrete actuators. Besides explicit damping augmentation, standard classical and modern feedback control methods have been proposed to maneuver flexible structures. A classical proportional-integral-derivative (PID) controller utilizing collocated actuator–sensor pairs was used by Dougherty et al. [8]. Cannon and Schmitz [9] utilized a non-collocated controller having torque input at the hub and an optical position sensor at the tip of the flexible members to actively control both the rigid-body angle and the vibration of a flexible system.

In recent years, there has been a considerable body of research on input command shaping for rapid endpoint positioning of a structure with minimal residual vibration. Meckle and Seering [10] developed an input function composed of series of harmonics of ramped sinusoids that approaches the rectangular shape, but does not include the harmonics having significant spectral energy at the natural frequencies of the system. Önsay and Akay [11] implemented multi-switch bang–bang control on a one-link continuous system to drive the arm from an initial to a final position in the minimum time with the least residual vibrations. For the same purpose, Singer and Seering [12] used an impulse function, and Jayasuriya and Choura [13] used natural modes of a given system as an input function. Recently, William and Donogh [14] proposed a method to design an actuator required to position the remote load and, simultaneously to provide active vibration damping by absorbing the reflected wave.

There have been, however, few attempts to reduce residual vibration by designing the path itself. Residual vibration sustained after a positioning move freely oscillates with the initial conditions which are the position and velocity errors at the end of a move. This vibration results not only from the dynamic characteristics of system but also from the manipulator path between its two endpoints. Recently Parks [15] developed a method to effectively reduce the residual vibration by designing the path itself. They established a dynamic model to describe the dynamic behavior of a manipulator at first, taking into account all flexibilities of links and joints. Then, based upon this model, they optimized the path to reduce residual vibration of the endpoint by representing the path using a combined Fourier series and polynomial function. This method does

not need some observers and controllers usually used in closed-loop control strategies. In other words, the optimal path can be selected to reduce the residual vibration when the initial and final points of the endpoint are given only.

In this work, a method is presented to effectively reduce the residual vibration under some torque constraints. These constraints should be considered because the maximum torque is limited to a certain degree at actuators used in industrial robot manipulators. The optimized path under torque constraints is compared with the designed path that has been presented in the previous research work without torque constraints. To this end, we briefly summarized the previous work and proceed to design the path to reduce the residual vibration of the endpoint under torque constraints.

2. Dynamical modelling

2.1. Generalized co-ordinates

The link flexibility can be represented as the deformation relative to the selected body-fixed co-ordinates. In general, we use the assumed spatial mode function to describe the deformation. This mode function, as is well-known, can vary largely depending on the selection of the co-ordinates.

As shown in Fig. 1, link deformations are represented in two ways; one is with reference to the virtual link co-ordinate system (VLCS) (a) and the other is relative to the tangent co-ordinate system (b). Both co-ordinate systems are moving co-ordinates, but the position of the former co-ordinate system is dependent only on joint angles of the preceding links. For instance, the origin of the VLCS for link 2 depends only on the angle θ_1 and is irrelevant to the deformation of link 1, as shown in Fig. 1a. In contrast, the origin of the tangent co-ordinate system $O_2x_2y_2$ in Fig. 1b depends not only on θ_1 but also on the deformation $v_1(L_1)$ of the preceding link deformation. In general, the motion of a tangent co-ordinate frame is a function of deformations $v_i(L_i)$ of the preceding links as well as the joint angles. This is why the equations of motion with

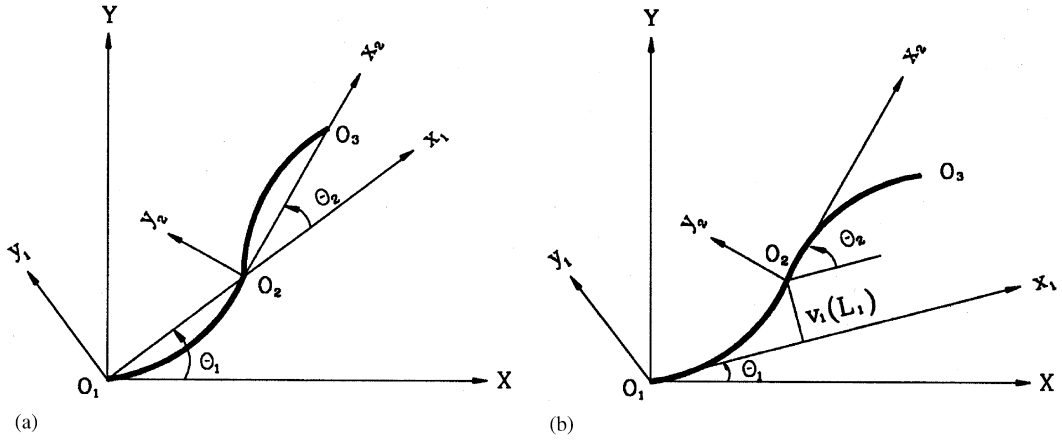

Fig. 1. A comparison of VLCS (a) and tangent co-ordinate system (b).

respect to the tangent co-ordinate systems are coupled with the deformations of the other links. The VLCS, on the other hand, is independent of the deformations of the other links. Thus the modelling by using the VLCS is an efficient way of formulating equations of motion in a compact form.

The mode functions to be used are dependent on the moving co-ordinates. When we adopt the tangent co-ordinate system as a moving co-ordinate, the mode functions used will be modes of a beam with one end fixed and the other free. This mode function has, as is well-known, a very complicated functional form. On the other hand, when we adopt the VLCS, we can use the mode functions of a simply supported beam as an assumed mode function. This function is very simple and easy to handle.

As a result, the VLCS is not only convenient for solving the dynamical equation, but also advantageous to reduce computational complexity. The boundary conditions that the link beams must satisfy are much simpler when the beam deformations are represented with respect to the VLCS. Also this co-ordinate representation allows us to compute dynamic equations for each link member independently from the others. If one can use a system of orthogonal functions the computation is further simplified, so that they can be divided into the ones in terms of individual generalized co-ordinate, separately.

2.2. Equations of motion

To formulate the dynamic equations of motion, we need to make assumptions on the construction of flexible arms discussed in this paper. We assume that the arm is planar, the open-loop linkage consisting of n links constrained in a horizontal plane.

In order to specify the configuration of a body, it is necessary to define a set of generalized co-ordinates. If we designate the axis $O_i x_i y_i$ as a co-ordinate system rigidly attached to ith link and the axis $O_{i-1}x_{i-1}y_{i-1}$ to $(i-1)$th link, the relative joint co-ordinates are specified by the relative angle θ_i between the $O_{i-1}x_{i-1}y_{i-1}$ axis and the $O_i x_i y_i$ axis. In addition to the generalized co-ordinates above, one needs generalized co-ordinates associated with link deformation. To this end, we first expand deformation $\mathbf{u}_i$ to a series of co-ordinates $\mathbf{q}_i^j$ by using the Rayleigh–Ritz functions for link i that satisfies conditions on independence and completeness, then the deformation $\mathbf{u}_i$ is written as

$$\mathbf{u}_i(x_i, t) = \sum_{j=1}^{s_i} \phi_i^j(x_i)\mathbf{q}_i^j(t). \tag{1}$$

In the above equation, ϕ_i^j is referred to as the assumed spatial mode function, and $\mathbf{q}_i^j$ as the time-varying mode amplitudes. Therefore, a vector of generalized co-ordinates of the ith body is defined by the set of relative co-ordinates θ_i and modal co-ordinate $\mathbf{q}_i^j$.

As shown in Fig. 2a, each joint of the manipulator is composed of an actuator, a transmission unit and an arm link. The elastic deformation of a joint is induced mainly by a transmission unit, because the elastic deformation of the gear teeth induces the joint flexibility. Therefore we model the joint flexibility as an equivalent torsional spring k_i, neglecting the inertia of the actuator. A schematic diagram of a representative joint having an equivalent torsional spring is shown in Fig. 2b.

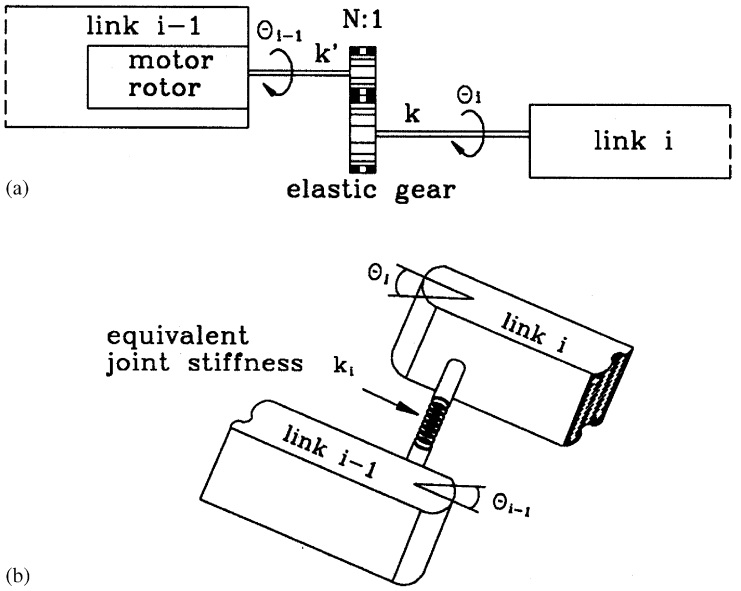

Fig. 2. Schematics of a flexible joint model: (a) joint mechanism; (b) compliant joint model.

The equation of motion of the physical system under consideration can be derived from the well-known Lagrangian equation. By substituting the kinetic energy, the potential energy and the generalized external force through tedious calculations, into the Lagrangian equation, we can derive the non-linear differential equations of motion for the flexible manipulator:

$$\mathbf{D}(\mathbf{X})\ddot{\mathbf{X}} + \mathbf{C}(\mathbf{X})\dot{\mathbf{X}} + \mathbf{K}\mathbf{X} + \mathbf{H}(\mathbf{X}, \dot{\mathbf{X}}) = \mathbf{T}, \tag{2}$$

where $\mathbf{D}(\mathbf{X})$ is the time-varying inertia matrix, $\mathbf{C}$ and $\mathbf{H}$ represent the Coriolis, centrifugal, elastic and centrifugal stiffening effects. $\mathbf{K}$ is the stiffness matrix, and $\mathbf{T} = [\tau_1 \quad \tau_2 \quad 0 \quad \dots \quad 0]^{\mathrm{T}}$ denote the generalized external vector. The generalized co-ordinate $\mathbf{X}$ is given by $\mathbf{X} = [\theta_1 \quad \theta_2 \quad q_1^1 \dots q_1^{s1} \quad q_2^1 \dots q_2^{s2}]^{\mathrm{T}}$.

2.3. Characteristics of residual vibration

Residual vibration sustained after a positioning move, freely oscillates with the natural frequencies of the final location and initial conditions which are the displacement and velocity errors at final time t_f. In opposition to the positioning motion, residual vibration performs small oscillations about the final location which can be regarded as an equilibrium configuration. Also residual motion is so slow that Coriolis and centrifugal effects, which make the equations of motion non-linear, can be neglected. Therefore we can linearize the equations of motion after the positioning move.

Suppose that the manipulator performs small oscillations about the final configuration specified by θ_{kf}. One writes

$$\theta_k(t) = \theta_{kf} + \theta_{ke}(t), \tag{3}$$

where $\theta_{ke}(t)$ denotes the small oscillations, and $|\theta_{ke}(t)| \ll 1$. In particular, it is assumed that one can make the approximations.

$$\cos\theta_{ke} \cong 1, \quad \sin\theta_{ke} \cong \theta_{ke}. \tag{4}$$

Therefore, we can write

$$\sin\theta_k = \sin(\theta_{kf} + \theta_{ke}) \cong \sin\theta_{kf} + \theta_{ke}\cos\theta_{kf} \tag{5}$$

and analogously

$$\cos\theta_k \cong \cos\theta_{kf} - \theta_{ke}\sin\theta_{kf}. \tag{6}$$

In addition, it is assumed that the motion of the manipulator about the equilibrium configuration is so slow that the products of the velocities, like the $\dot{\theta}_{ke}^2$ and $\dot{\theta}_{ke}q_k$ etc., can be neglected in the equations of motion. It is also assumed that terms such as $\theta_{je}\ddot{\theta}_{ke}$ can be ignored because of the same reason. If one makes the approximations suggested in Eqs. (3)–(6), then one can reduce the basic Eq. (2) to the following linearized systems of equations of motion:

$$\mathbf{D}(\theta_{kf})\ddot{\mathbf{X}}_e + \mathbf{K}\mathbf{X}_e = 0. \tag{7}$$

Comparing Eq. (7) with Eq. (2), it is seen that the vector **H** which makes the equations of motion non-linear has been eliminated. The inertia matrix **D** is not time-variant any longer. If θ_{kf} is defined, **D** becomes constant.

The response of the linearized system (7) can be easily obtained by using modal analysis:

$$\mathbf{X}_e(t) = \sum_{p=1}^{N}(\mathbf{w}_p^{\mathrm{T}}[D]\mathbf{X}_e(0)\cos\omega_p t + \mathbf{w}_p^{\mathrm{T}}[D]\dot{\mathbf{X}}_e(0)\frac{1}{\omega_p}\sin\omega_p t)\mathbf{w}_p, \tag{8}$$

where $\mathbf{X}_e(0)$ and $\dot{\mathbf{X}}_e(0)$ is the initial condition vector which is the displacement and velocity errors at the final location as explained in Eq. (8). Also ω_p is the pth natural frequency and $\mathbf{w}_p$ is the pth mode vector.

The tip position of two-link manipulator is given by

$$\begin{aligned} x &= L_2\cos(\theta_1 + \theta_2) + L_1\cos\theta_1, \\ y &= L_2\sin(\theta_1 + \theta_2) + L_1\sin\theta_1. \end{aligned} \tag{9}$$

Substituting Eqs. (3)–(6) into Eq. (9) and rearranging them, the tip position error during the residual vibration is written as

$$\begin{aligned} x_e &= -L_2(\theta_{1e} + \theta_{2e})\sin(\theta_{1f} + \theta_{2f}) - L_1\theta_{1e}\sin\theta_{1f}, \\ y_e &= -L_2(\theta_{1e} + \theta_{2e})\cos(\theta_{1f} + \theta_{2f}) - L_1\theta_{1e}\cos\theta_{1f}. \end{aligned} \tag{10}$$

The relation between the tip position error and the final location error can be obtained by substituting θ_{1e}, θ_{2e} of Eq. (8) into Eq. (10):

$$\begin{aligned} x_e &= \textstyle\sum_{p=1}^{N} C_p\cos(\omega_p t - \phi_p), \\ y_e &= \textstyle\sum_{p=1}^{N} D_p\cos(\omega_p t - \phi_p), \end{aligned} \tag{11}$$

where C_p and D_p are the amplitudes of the time-varying positioning errors and can be represented as $C_p, D_p = C_p, D_p(\theta_{kf}, \mathbf{w}_p, \omega_p, \mathbf{X}_e(0), \dot{\mathbf{X}}_e(0))$. The absolute value of the position error is defined as $p_e = \sqrt{x_e^2 + y_e^2}$. The constants C_p, D_p are functions of the final location error, and decrease when

this error has a smaller value. Hence the tip position error becomes smaller as this final location error decreases.

The ratio of the joint angle error, $\theta_{er} = (\theta_{2e}(0)/\theta_{1e}(0))$, for minimizing the position error p_e, can be obtained by

$$\frac{\partial p_e}{\partial \theta_{er}} = 0. \tag{12}$$

From Eq. (12), neglecting the errors of mode co-ordinates which are much smaller than the errors of joint angle, we can derive the ratio of the joint angle error of the two-link manipulator which minimizes the tip position error. The result is $\theta_{er} = w_{22}$ where w_{22} is the (2,2) element of the modal matrix.

The three-dimensional plot of the absolute value of the tip position error is drawn in Fig. 3a, to the variations of the magnitude and the ratio of the joint angle error. It is seen that the tip position error decreases overall as the magnitude of the joint angle error becomes smaller. It is also found that the ratio of the joint angle error has a considerable effect on the tip position error. Even when the magnitude of the joint angle error is constant, the tip position error varies depending on the

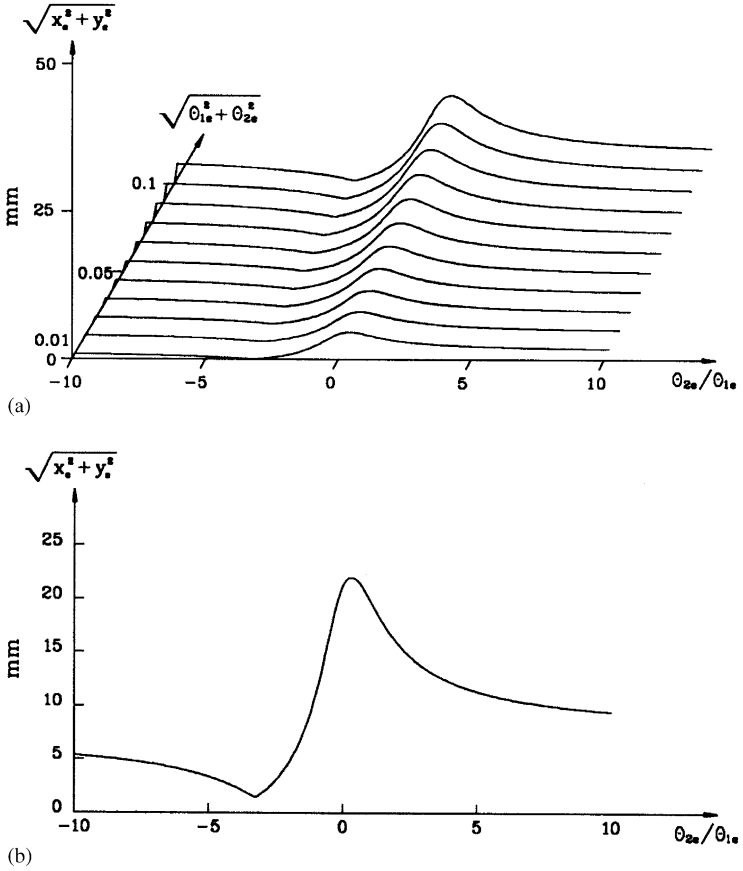

Fig. 3. Tip position error versus magnitude and ratio of joint angle error (a) and tip position error versus ratio of joint angle error for a magnitude of joint angle error, 0.05 (b).

ratio of the joint angle error. In Fig. 3b, the tip position error is plotted to the variation of the ratio of the joint angle error having the same magnitude, 0.05. As shown in the figure, the tip position error is heavily dependent on the ratio of the joint angle error as well. From the simulation results, it was found that the tip position error has a minimum value at $\theta_{er} = -3.26$, which is the same value as the (2,2) element of the modal matrix. From the results above we can see that the residual vibration of the arm tip is dependent, not only on the magnitude of the joint angle error, but also on the ratio of this error.

3. Path optimization

3.1. Performance index

From the previous results [15], the amplitude of the residual vibration can be minimized: both when the magnitudes of the error of the joint displacements and velocities at the final time is smaller, and when the ratio of these errors satisfies a certain criterion. Therefore, one cannot reduce the residual oscillations of the manipulator only by minimizing the absolute value of the final location error. In this paper the performance index to be minimized is chosen as the maximum value of the tip position error during the residual vibration:

$$J = \max p_e \quad \left(p_e = \sqrt{x_e^2 + y_e^2} \text{ for } t \geqslant t_f \right). \tag{13}$$

The performance index in the above equation can be obtained by numerical integration of the equations of motion. Consequently, we need the dynamic equations derived in Eq. (2) to formulate the optimization problem. Also the kinematic constraints should be satisfied at both ends:

$$\Theta_i = \Theta_{id}, \quad \dot{\Theta}_i = 0, \quad \ddot{\Theta}_i = 0 \quad \text{at} \quad t = 0, t_f, \tag{14}$$

where Θ_i, $\dot{\Theta}_i$ and $\ddot{\Theta}_i$ are the kinematic joint angle, joint velocity and joint acceleration and Θ_{id} is the required joint angle.

From the previous results, it was observed that most motion takes place in the first half of duration, so that higher torques are needed. The actuators used in industrial robot manipulators for driving robot arms, however, is limited in the maximum torque which they can exert. Therefore we need the constraints for the actuator torques. That constraints can be written as follows:

$$\tau_{min} \leqslant |\tau_i| \leqslant \tau_{max} \quad i = 1, 2, \ldots, n. \tag{15}$$

It is the purpose of this paper to find the optimal tip path satisfying the above optimality condition. Hence, we can define the design variables as the each joint trajectories that make the optimal path of the arm tip.

3.2. Functional development of path

In order to formulate the optimal design problem, we need the functional development of the each joint trajectory. Fourier and polynomial approximation techniques are commonly used in

the functional expansion of generalized co-ordinates. A polynomial function exactly satisfies the boundary conditions, but contains the unwanted higher harmonics that excite the system resonance. Another demerit of this polynomial function is that we cannot assure the convergence of the solution by increasing the terms of the polynomials. On the other hand, a Fourier series expansion has opposite characteristics: guarantees of convergence by adding terms and dissatisfactions of boundary conditions. So we propose the approximation method of the each joint trajectory to combine the advantages of the two functions.

Any joint trajectory can be expanded by a finite cosine Fourier series using a half range expansion:

$$\theta_i(t) = a_{i0} + \sum_{m=1}^{M} a_{im} \cos \frac{m\pi}{t_f} t. \tag{16}$$

This approach, however, has the following disadvantages:

(1) Convergence is guaranteed only in $(0, t_f)$. To satisfy the requirements on arbitrary conditions, convergence should be extended from $(0, t_f)$ to $[0, t_f]$.
(2) Although $\theta_i(t)$ converges to the optimal solution, there is no guarantee that the derivative of $\theta_i(t)$ will converge to the derivative of the optimal solution.
(3) The rate of convergence of the Fourier series depends on the optimal solution. This rate can be quite slow.

To overcome these disadvantages, we approximate each of the joint co-ordinates by the sum of a fifth order polynomial and a finite-term Fourier series.

$$\theta_i(t) = \lambda_i(t) + \sigma_i(t), \tag{17}$$

where

$$\lambda_i(t) = \sum_{j=0}^{5} \lambda_{ij} t^j, \quad \sigma_i(t) = \sum_{m=1}^{M} a_{im} \cos \frac{m\pi}{t_f} t.$$

Here, the constant term of the Fourier series has been included in the fifth order polynomial, $\lambda_i(t)$.

The boundary condition requirements can be written as

$$\begin{aligned}
&\theta_i(0) = \lambda_i(0) + \sigma_i(0),\\
&\theta_i(t_f) = \lambda_i(t_f) + \sigma_i(t_f),\\
&\dot{\theta}_i(0) = \dot{\lambda}_i(0) + \dot{\sigma}_i(0),\\
&\dot{\theta}_i(t_f) = \dot{\lambda}_i(t_f) + \dot{\sigma}_i(t_f),\\
&\ddot{\theta}_i(0) = \ddot{\lambda}_i(0) + \ddot{\sigma}_i(0),\\
&\ddot{\theta}_i(t_f) = \ddot{\lambda}_i(t_f) + \ddot{\sigma}_i(t_f).
\end{aligned} \tag{18}$$

These equations can be used to determine the coefficients of the polynomial in terms of the coefficients of the Fourier series and the boundary values. Solving the above boundary condition equations gives the following closed-form expression of the six coefficients:

$$\lambda_{ij} = \lambda_{ij}(a_{im}, \text{ boundary value of } \theta_i, \dot{\theta}_i, \ddot{\theta}_i). \tag{19}$$

Therefore, we can remedy the disadvantages of the Fourier series expansion, not increasing the number of terms to be designed. Also, the boundary conditions can be embedded naturally in the approximation to eliminate the kinetic requirements at both ends. The design variables are the coefficients of the Fourier series, a_{im} $(m = 1, 2, \ldots, M)$.

If the design variables a_{im} are determined, the joint displacements, velocities and accelerations can be obtained by Eq. (17). Then the required torques to track the desired trajectory can be computed by the inverse dynamics. Applying these torques to the flexible dynamic equations, the dynamic responses of the flexible manipulator can be numerically obtained. From these results, we can compute the value of the performance index in Eq. (13). If this value cannot satisfy the optimality criterion, the optimization routine iterates by adjusting the design variables a_{im} until the minimum point is reached.

3.3. Selection of design variables

In Section 3.2, each joint trajectory was functionally developed by the combined polynomial and finite-term cosine Fourier series. But still the joint trajectories are expanded by all the sequential Fourier series up to the highest harmonic number. In that case, it is unavoidable that some Fourier coefficients which have a negligible contribution to the reduction of residual vibration are included in the expansion. Thus if we take all the terms up to the highest harmonic number, the computation efficiency becomes worse. In general the accuracy of the optimal solution can be increased and its computing time can be greatly reduced, if we can remove the less contributing terms. For this reason, a technique to remove the less contributing terms in the combined Fourier series expansion is required.

The concept of correlation coefficients can be used to select the necessary Fourier terms as follows. The correlation coefficients between the x position error of the arm tip, x_e and mth harmonic function of Fourier series, $\sigma_m = \cos(m\pi t/t_f)$ are defined as follows:

$$\rho_{x_e\sigma_m} = \frac{S_{x_e\sigma_m}}{S_{x_e x_e} S_{\sigma_m\sigma_m}} = \frac{\sum_{k=1}^{N_d} x_e(k)\sigma_m(k)}{\sqrt{\sum_{k=1}^{N_d} x_e^2(k) \sum_{k=1}^{N_d} \sigma_m^2(k)}}. \tag{20}$$

The correlation coefficients between the y position error and the mth harmonic function, $\rho_{y_e\sigma_m}$ can be defined analogously. The correlation coefficient $\rho_{x_e\sigma_m}$ defined in Eq. (20) will lie between -1 and $+1$. And if the absolute value of it is in the vicinity of 1, it means that the correlation between x_e and σ_m is high and σ_m should be included in the expansion of the joint co-ordinates. In contrast, if the absolute value is near 0, σ_m can be excluded in the expansion.

$\rho_{x_e\sigma_m}$ has a different acceptance region according to the level of significance:

$$\frac{\sqrt{N_d - 3}}{2}\left|\ln\left[\frac{1 + \rho_{x_e\sigma_m}}{1 - \rho_{x_e\sigma_m}}\right]\right| \geqslant z_{\alpha/2}, \tag{21}$$

where N_d is the number of the sampling data, z is the standardized normal variable, and α is the level of significance. If $\rho_{x_e\sigma_m}$ satisfies the above inequality, we can say that a correlation exists between x_e and σ_m at the α level of significance. The same theory can be applied to $\rho_{y_e\sigma_m}$. Therefore, we can greatly reduce the number of design variables by selecting the harmonic functions satisfying inequality (21) only.

4. Results and discussion

The optimal path is designed for the two-link manipulator to evaluate the proposed approach. In order to analyze the dynamic response of the flexible manipulator, parameters such as mass, stiffness and Young's modulus must be provided. The arm construction we considered consists of rectangular aluminum beams of 1 m length each. The mass is 3.5 kg, the dimension of the cross-section is 3×4 cm, and Young's modulus is 7.1×10^3 kgf/mm^2. The joint spring constant is 2 kN m/rad. The order of mode function is $s_1 = s_2 = 3$ for each links. The duration time is 1 s. The manipulator starts its motion at $\theta_{10} = -90^\circ$, $\theta_{20} = 90^\circ$ and ends at $\theta_{1f} = 0^\circ$, $\theta_{2f} = 45^\circ$.

The initial path is chosen as the cycloidal motion. The motion of the arm tip for cycloidal function is shown in Fig. 4. Cycloidal motion is one of the very smooth types of motion, largely used in the design of the cam profile. The actuator torques of the rigid manipulator required to track the desired trajectory can be found by the inverse dynamics. To evaluate the effects of the flexibility, a time series of computed torques are plugged into the flexible dynamic equations. The tracking errors and residual vibrations of the arm tip will be shown and discussed in later part of this chapter, compared with the optimized results.

Residual vibrations are composed of the tip position error in the x and y directions. The correlation coefficients between the x and y position error of the arm tip for the cycloidal motion and the harmonic functions of the Fourier series are shown in Fig. 5. If the number of data is 50, the correlation coefficients should be higher than 0.35 at the level of significance $\alpha = 0.01$ to satisfy Eq. (21). Only the third and fourth harmonic function in the x direction error, and the fourth, fifth, sixth in the y direction error satisfy this criterion. These harmonic numbers are equal

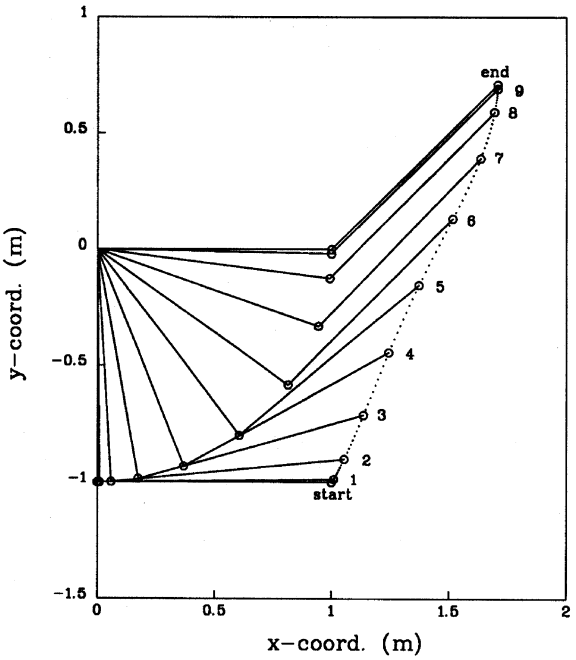

Fig. 4. Arm motion and tip path for cycloidal motion.

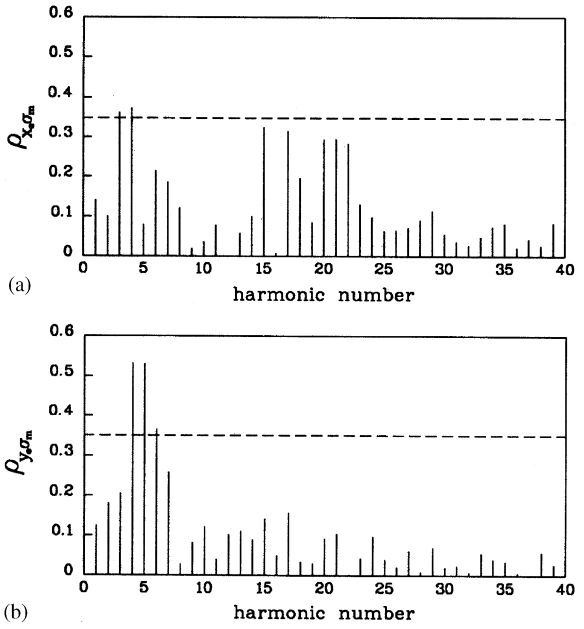

Fig. 5. Correlation coefficients of tip position error for cycloidal motion: (a) x-position error; (b) y-position error.

to the variation of the first natural frequency of the system. Therefore the manipulator path can be developed by using only the 3, 4, 5 and 6th harmonic functions of the Fourier series and polynomial function without serious errors. Needless to say, the computation efforts can be greatly reduced when each joint trajectory is expanded by only 4 terms. The constraints for maximum torque are set at 100 and 60 N m, respectively. The maximum torque, 60 N m, is equivalent to the maximum torque for cycloidal motion.

4.1. Optimized path without torque limits

The optimally designed tip path is shown in Fig. 6. In this case we set no limits for the maximum torques. First of all, we can see that the optimized path is much different from the cycloidal motion which has a nearly straight tip path. It is seen from Fig. 6 that Link 1 exhibits a fast motion and Link 2 displays a clear inward motion during the first half of the path. This is in the opposite direction of the cycloidal motion, comparing Fig. 6 with Fig. 4. After Link 1 has almost completed its move, Link 2 moves outwards to the required final position. This means that most of the motion is accomplished in the first half; and in the second half, the arm tip approaches the final position compensating for the position errors caused by the fast motion.

To evaluate the difference, the optimized path and computed torques are plugged into the dynamic equations derived in Eq. (2). The tracking errors and residual vibrations of the arm tip in the x, y directions are shown in Fig. 7 compared with those results for the cycloidal motion. As shown in the figure, the optimized path results in a very small residual vibration, while cycloidal motion yields a relatively large vibration. This can be more obviously seen in Fig. 8, in which the residual vibration of the arm tip is plotted in space co-ordinates. The maximum amplitudes of the

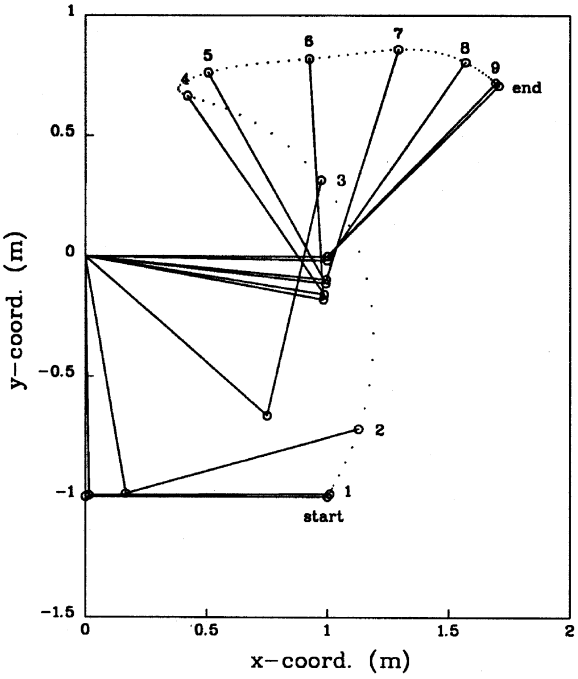

Fig. 6. Arm motion and tip path for unlimited optimal motion.

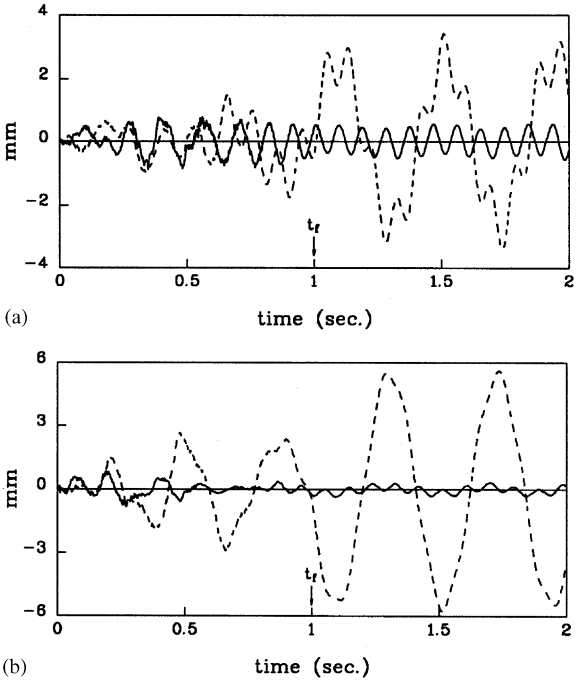

Fig. 7. Tip position error for cycloidal (dashed) and unlimited optimal motion (solid): (a) x-position; (b) y-position.

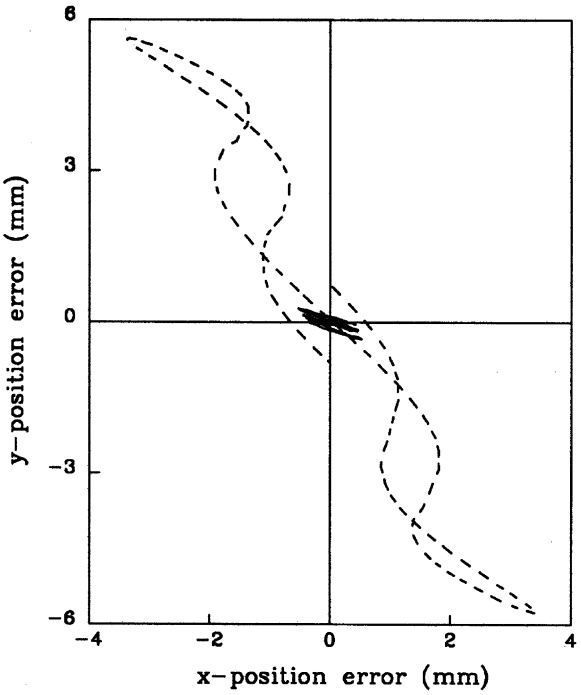

Fig. 8. Residual vibration of arm tip for cycloidal (dashed) and unlimited optimal motion (solid).

residual vibration are 3.43 mm in the x direction and 5.75 mm in the y direction for the cycloidal motion, while it reduces to 0.56 mm in the x direction and 0.34 mm in the y direction for the optimized path. The maximum amplitudes are significantly lower, only 16.3 percent of the maximum amplitude for the cycloidal motion in the x direction and only 5.9 percent in the y direction.

The prominent frequency components of the residual vibration for the cycloidal motion are 2.36 and 10.82 Hz. The addition of the frequency components around the first frequency, 2.36 Hz, drastically reduces the magnitude of this frequency in the residual vibration for the optimized path. Physically, this means that optimized path developed by the Fourier series (including these frequency components) offsets the occurrence of the oscillation with these frequencies. This fact can be assured by the results that the residual vibration in the y direction, in which the first frequency component is more prominent, is largely reduced compared to the x direction.

4.2. *Optimized path under torque limits*

The results in Section 4.1 are for the unlimited optimal path, in which the maximum torque for driving the manipulator arms is 4 times large as that of cycloidal motion. In this section, we design the optimal path under some torque constraints and compare it with the path designed under no torque constraints. When the maximum torque is limited by 100 N m, we can obtain the optimal path as shown in Fig. 9. The shapes of the input torques are similar to the unlimited case, but we can see from Table 1 that the maximum torque is limited by 98.306 N m for actuator 1. From the

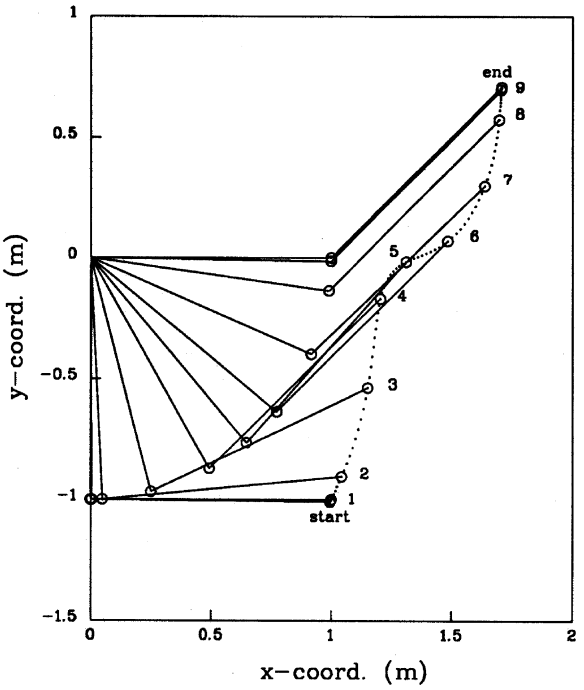

Fig. 9. Arm motion and tip path for torque-limited optimal motion, $|\tau_i| < 100$.

Table 1
A comparison of maximum torque

	Cycloidal	Unlimited optimal path	Torque-limited optimal path ($|\tau_i| < 100$)	Torque-limited optimal path ($|\tau_i| < 60$)
$|\tau_1|$	57.859	233.334	98.306	59.829
$|\tau_2|$	11.786	80.878	33.114	12.123

results it is found that the tip path tries to follow the unlimited path but returns to the target position without completing the motion developed in unlimited path, due to the torque constraints. The residual vibration of the arm tip for the torque-limited path is shown in Fig. 10. It can be seen that the magnitude of residual vibration becomes larger compared with the unlimited case, especially in the x direction. The vibration in the y direction remains almost unchanged. From Table 2, it can be seen that the maximum amplitudes of position error is 27.8 percent of that for cycloidal motion in the x direction, and 7.8 percent in the y direction.

The optimized path in which the maximum torque is limited by 60 N m is presented in Fig. 11. The torque limit, 60 N m, is equivalent to the maximum torque for cycloidal motion. The optimal path is very similar to that of cycloidal motion because the torque limits for both cases are almost same as shown in Table 1. The magnitudes of residual vibration for this path are larger than those of the unlimited path and torque-limited path ($|\tau_i| < 100$) as shown in Fig. 12. It is, however, seen that the position errors are smaller than those for cycloidal motion yet. This is due to the fact that

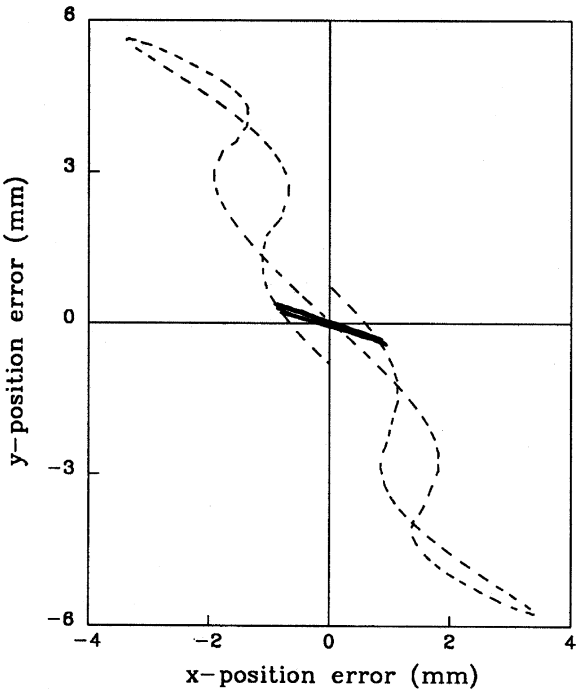

Fig. 10. Residual vibration of arm tip for cycloidal (dashed) and torque-limited optimal motion (solid), $|\tau_i| < 100$.

Table 2
A comparison of maximum position error

	Cycloidal	Unlimited optimal path	Torque-limited optimal path ($|\tau| < 100$)	Torque-limited optimal path ($|\tau| < 60$)
x_e	3.4326	0.5628	0.9557	1.1354
y_e	5.7585	0.3367	0.4482	1.1852

although the maximum torque is limited by same value, the residual vibration can be reduced when the magnitudes of position errors is decreased at final time t_f and the ratio of these errors satisfies the optimal value.

5. Conclusions

A method was presented for generating the path of a flexible manipulator under torque constraints, which significantly reduces residual vibration. This is based on an optimized path that has been constructed from a combined Fourier series and polynomial, with coefficients of each harmonic term selected to minimize the residual vibration. In modelling the dynamics of a flexible

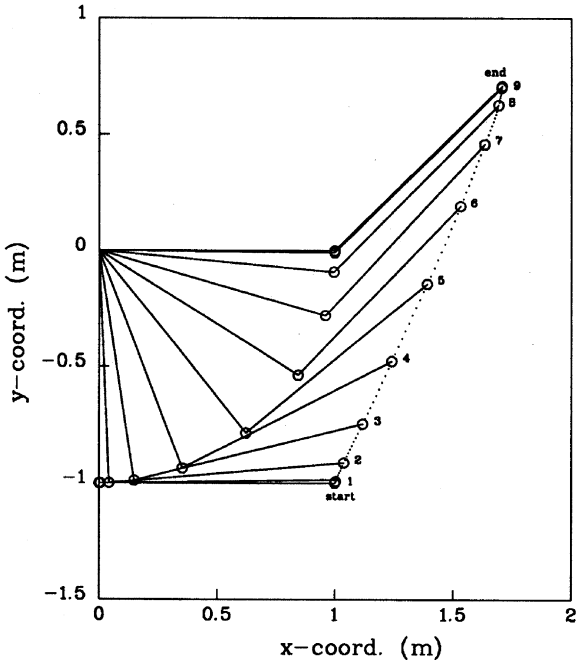

Fig. 11. Arm motion and tip path for torque-limited optimal motion, $|\tau_i| < 60$.

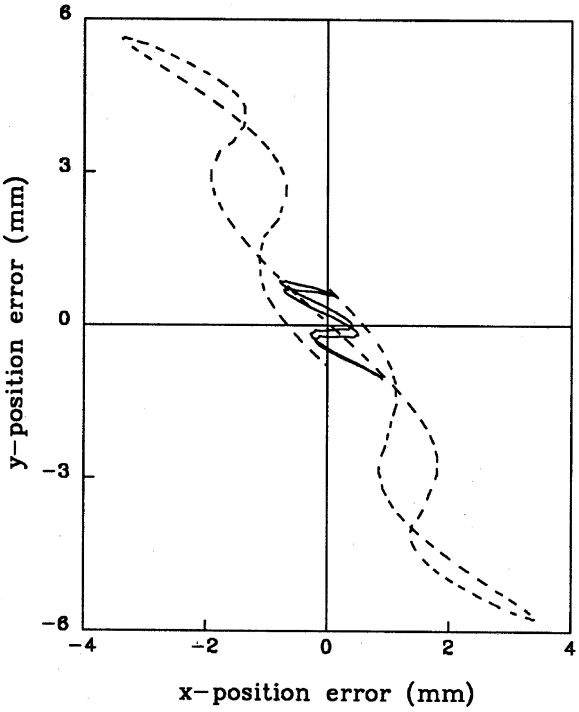

Fig. 12. Residual vibration of arm tip for cycloidal (dashed) and torque-limited optimal motion (solid), $|\tau_i| < 60$.

arm, the virtual link co-ordinates are used. These co-ordinates are not only convenient for modelling and optimization, but also advantageous for reducing computational complexity.

The manipulator path was developed by a combined Fourier series and polynomial. This expansion satisfies both the guarantees of convergence by adding terms and the matching of the boundary conditions. The concept of correlation was used to select the minimum number of design variables, i.e., Fourier coefficients, only contributing to the reduction of the residual vibration, which largely reduces the computing time.

The optimization algorithm has been applied to a two-link planar manipulator. Through simulation, the efficiency and usefulness of the optimized path were shown. Regardless of the torque constraints, the optimized path produced motion with considerably lower residual vibration compared to a cycloidal motion. For the case of unlimited optimal path, the magnitude of residual vibration reduces by 90.2 percent, and 84.2, 75.7 percent for the torque-limited cases, respectively. From these results, it can be concluded that even the input torques are limited, the residual vibration of a flexible manipulator could be drastically reduced by selecting an appropriate path.

References

[1] D.M. Aspinwall, Acceleration profiles for minimizing residual response, *Journal of Dynamic Systems, Measurements and Control* 102 (1980) 3–6.

[2] H. Sehitoglu, J.H. Aristizabal, Design of a trajectory controller for industrial robots using bang-bang and cycloidal motion profiles, *American Society of Mechanical Engineers, Winter Annual Meeting*, 1986, pp. 169–175.

[3] C.J. Swigert, Shaped torque techniques, *Journal of Guidance and Control* 3 (1980) 460–467.

[4] J.D. Turner, H.M. Chun, Optimal distributed control of a flexible spacecraft during a large-angle manoeuver, *Journal of Guidance and Control* 7 (1984) 257–264.

[5] A. Hanafi, F.W. Wright, Optimal trajectory control of robotic manipulators, *Mechanism and Machine Theory* 19 (1984) 267–273.

[6] T.E. Alberts, G.G. Hastings, W.J. Book, S.L. Dickerson, Experiments in optimal control of a flexible arm with passive damping, *Proceedings of the Fifth VPI & SUAIAA Symposium on Dynamics and Control of Large Structures*, 1985, pp. 423–435.

[7] L.M. Sliverberg, Uniform damping control of spacecraft, *Journal of Guidance, Control and Dynamics* 9 (1986) 221–227.

[8] H. Doughrty, K. Tompetrini, J. Levinthal, G. Nurne, Space telescope pointing control system, *Journal of Guidance, Control and Dynamics* 5 (1982) 403–409.

[9] R.H. Cannon, E. Schmitz, Initial experiments on the end-point control of a flexible one-link robot, *International Journal of Robotics Research* 3 (1984) 62–75.

[10] P.H. Meckl, W.P. Seering, Minimizing residual vibration for point-to-point motion, *Journal of Vibration, Acoustics and Stress Reliability in Design* 107 (1985) 378–382.

[11] T. Önsay, A. Akay, Vibration reduction of a flexible arm by time-optimal open-loop control, *Journal of Sound and Vibration* 147 (1991) 283–300.

[12] N.C. Singer, W.P. Seering, Pre-shaping command inputs to reduce system vibration, *Journal of Dynamic Systems, Measurements and Control* 112 (1990) 76–82.

[13] S. Jayasuriya, S. Choura, On the finite settling time and residual vibration control of flexible structures, *Journal of Sound and Vibration* 148 (1991) 117–136.

[14] O. William, L. Donogh, Position control of flexible robot arms using mechanical waves, *Journal of Dynamic Systems, Measurements and Control* 120 (1998) 334–339.

[15] K.J. Park, Y.S. Park, Fourier-based optimal design of a flexible manipulator path to reduce residual vibration of the endpoint, *Robotica* 11 (1993) 263–272.